Electrochemical conversion of CO_2 plasmas

Haytham E. M. Hussein,[a,d] Panagiotis N. Kechagiopoulos,[b] Angel Cuesta[a,c]

[a]Advanced Centre for Energy and Sustainability (ACES), School of Natural and Computing Sciences, University of Aberdeen, AB24 3UE Aberdeen, Scotland, UK; [b]Chemical Processes & Materials Group, School of Engineering, University of Aberdeen, Aberdeen AB24 3UE, UK; [c]Instituto de Química Física Blas Cabrera, CSIC, C. Serrano 119, E-28006 Madrid, Spain

[d]GSK Carbon Neutral Laboratories for Sustainable Chemistry, Jubilee Campus, Wollaton Road, University of Nottingham, Nottingham, NG8 1BB, UK

Table of contents

S1: Images of the catalysts used during the electrochemical conversion of CO_2 and CO_2 NTP

The SEM images in Fig. S1(ai and aii) reveal the structure of the cathode, depicting CuO nanoparticles dispersed on the GDE surface and the anode composed of IrO_2 (Fig. S1(b)). Fig. S1 (c) and (d) show the energy-dispersive X-ray spectroscopy (XEDS) data of the corresponding catalyst.

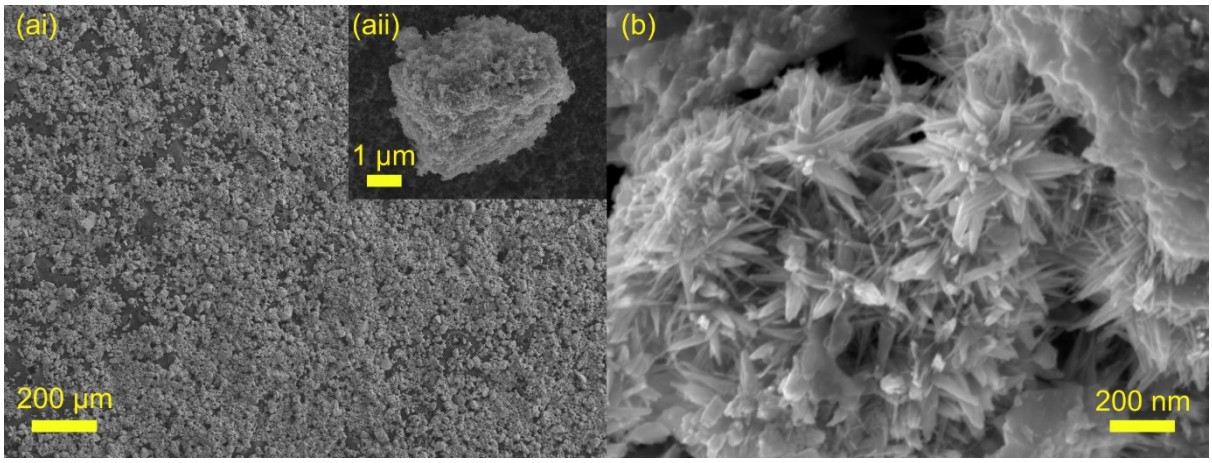

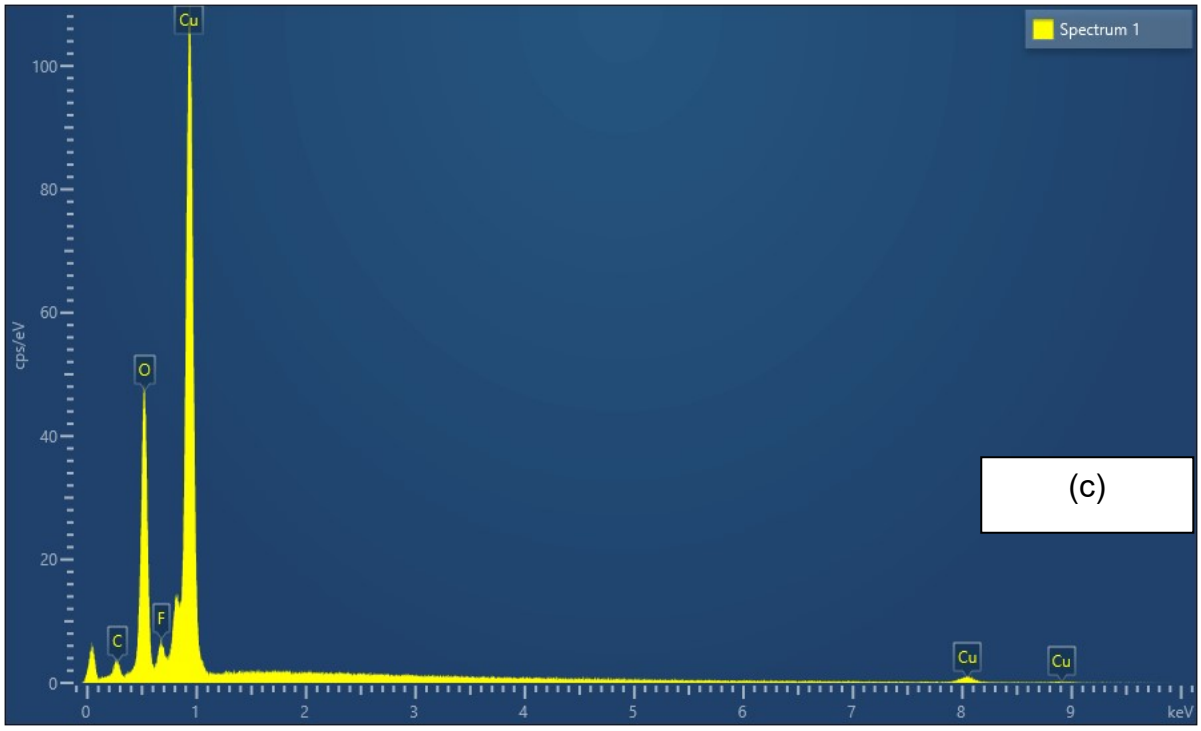

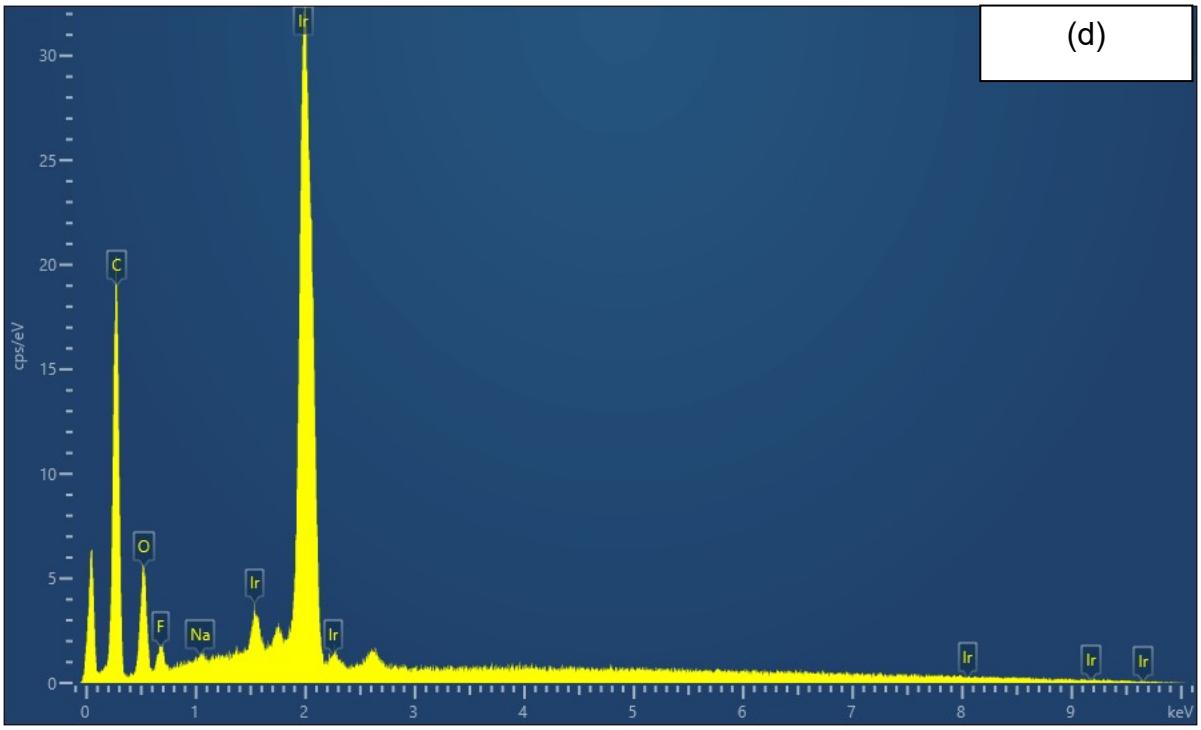

Figure S1: SEM images of the cathode (ai), the inset is a zoom into one of the CuO nanoparticles(aii) and the anode is made of IrO_2 nanoparticles (b). XEDS spectrum of CuO (c) and IrO_2 (d).

S2: 3D CAD drawing and images describing the components of the electrolyte-gap electrolyser when integrated with the CO_2 plasma source

The 3D CAD schematic (Fig. S2(a)) and a photograph of the experimental setup (Fig. S2(b)) describe an electrolyte-gap electrolyser optimised for CO_2 plasma integration. The plasma source introduces reactive species (*e.g.,* CO molecules or excited states, O radicals) or energetic electrons that lower the activation barrier for CO_2 reduction. This design aimed to combine efficient mass transport with plasma activation, which may explain the improved performance metrics in Figs. S9–S13. A rod tip-to-cathode distance of 10 mm was selected to ensure stable discharge operation without arcing and to facilitate reproducible integration with the cell. Future research will focus on the systematic optimisation of this distance, as it significantly influences post-discharge transport and the decay of excited species. Note that methanesulfonate (SO_3CH_3), also referred to as mesylate, is frequently employed in electrochemical CO_2 reduction (CO_2RR) as a "spectator" ion, indicating that it neither participates in reactions nor influences the catalyst.[1] Its chemical structure and electronic properties confer stability, with the sulfur atom in methanesulfonate existing in its highest oxidation state (+6). The reduction of this sulfur would necessitate the cleavage of strong bonds, requiring more energy than the reduction of CO_2 or water. Methanesulfonate exhibits stability across a broad range of potentials, exceeding those typically utilised for CO_2 reduction (approximately -1.5 V vs. RHE).[1] Unlike other sulfur-containing compounds, methanesulfonate possesses a robust carbon-sulfur bond that resists cleavage, thereby preventing the formation and adsorption of deleterious substances such as hydrogen sulfide on the catalyst.[2] Unlike bicarbonate, methanesulfonate does not react with CO_2 or its intermediates, serving solely to facilitate ionic conductivity.[2]

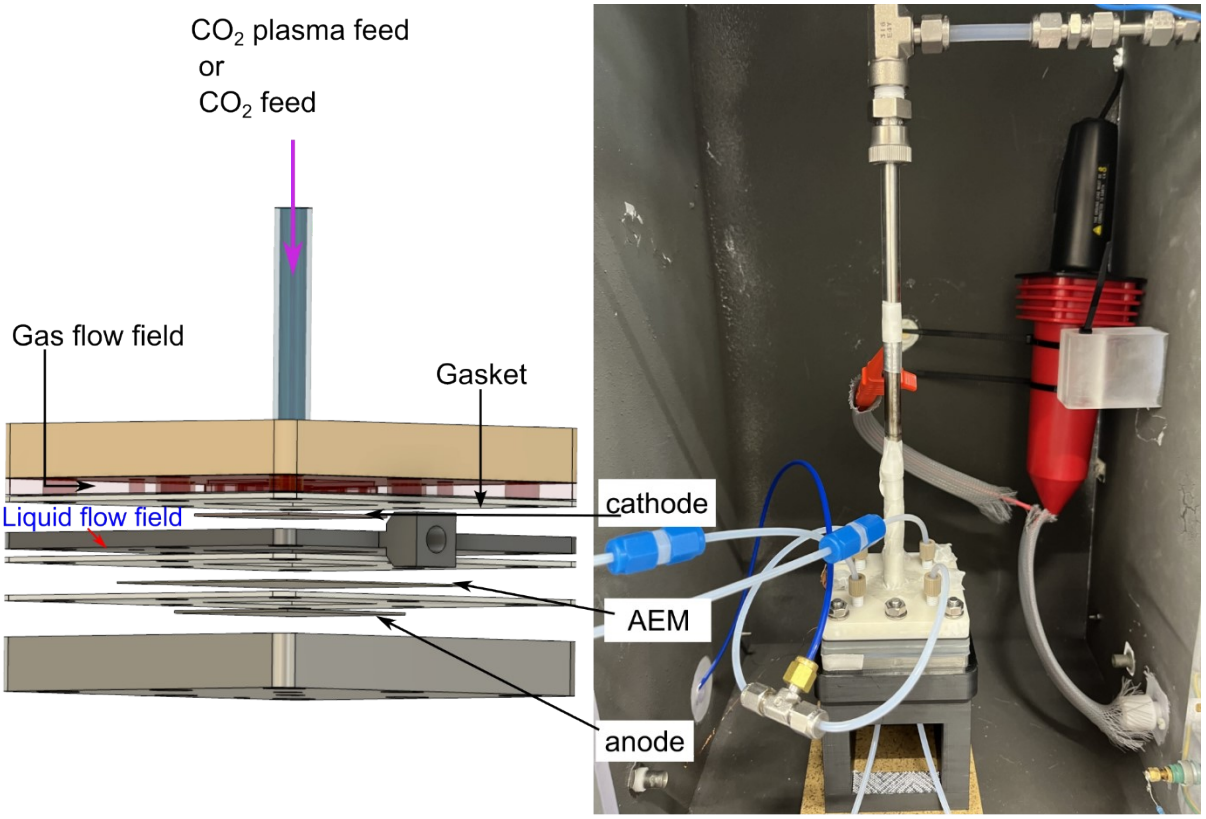

(a) A schematic presentation of the cell (b) A photograph of the experimental set-up

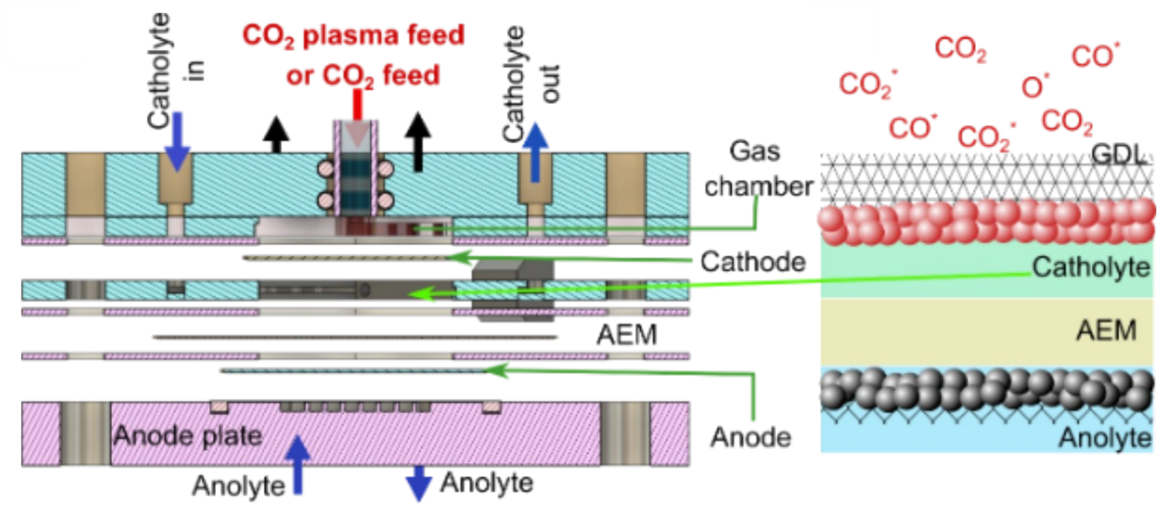

(c) A cross section and a schematic representation of the electrolyte-gap electrolyser

Figure S2: (a) Schematic representation and (b) a photograph of the electrolyte-gap electrolyser, with a catholyte flow field between the cathode and the AEM. There is no electrolyte gap between the AEM and the anode. The anolyte flows through a titanium flow plate at the back of the anode. (c) Cross-section and schematic representation of the electrolyte-gap electrolyser.

S3: CO_2 plasma power calculation and Optical emission spectroscopy

We calculated the plasma power by analysing the voltage and charge cycles from the experimental data using Lissajous figure analysis, as shown in Fig. S3, based on the voltage and charge signals, as shown in Fig. S4. The current was obtained in certain cases through a passive probe sampling the voltage across a resistor (68 Ω) placed on the ground line.

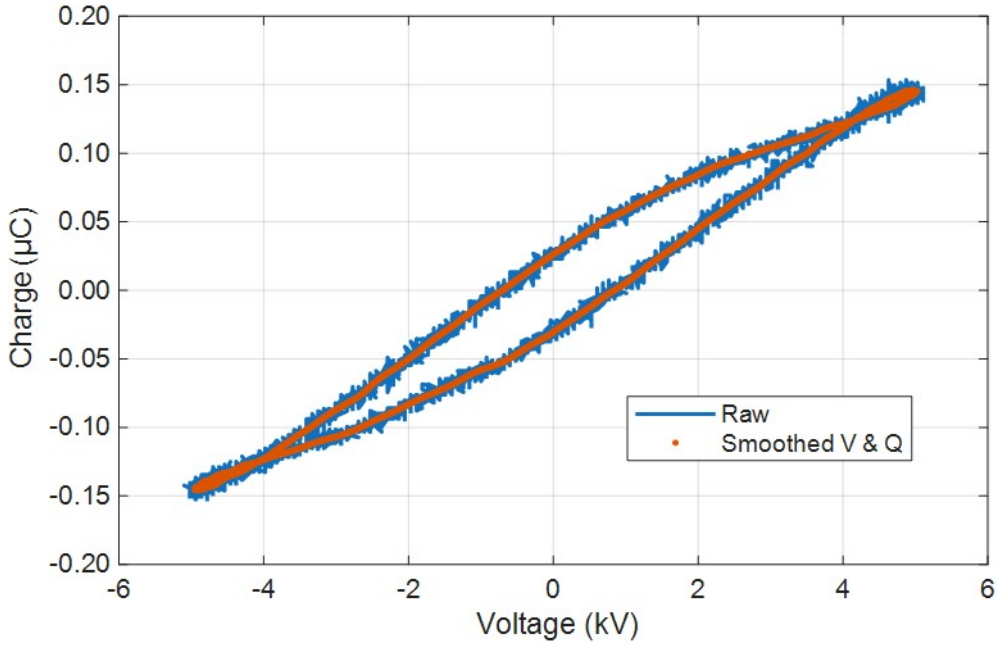

Figure S3: The Lissajous plot of the CO_2 DBD plasma

Figure S4: Current, charge, and voltage traces vs time

Optical emission spectroscopy (OES) analyses the populations of various species generated in CO_2 NTP DBD, including CO_2 vibrational states, O radicals, and CO

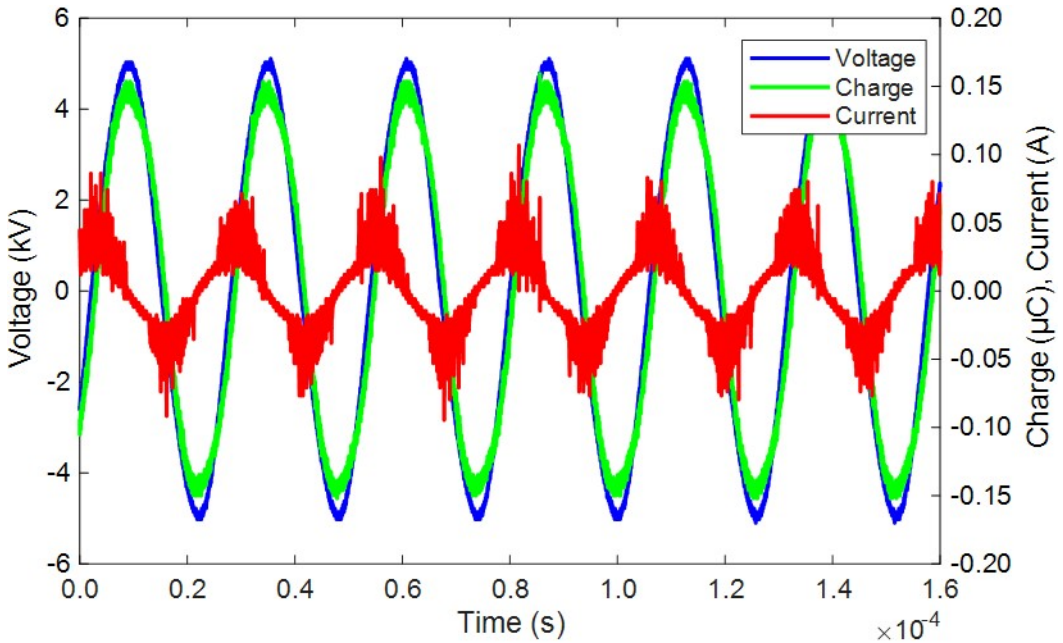

molecules, during non-thermal CO_2 plasma discharge (see Fig. S5 and Table SI1). The observed OES features align with previous studies on CO_2 dielectric barrier discharges, which typically display CO molecular bands, including the Ångström system, and CO_2^+ ultraviolet features, along with atomic oxygen lines depending on the dissociation conditions.[3] For instance, the CO Ångström emission near ~451 nm is commonly employed for CO_2 NTP DBD diagnostics, and CO_2^+ UV features around ~288–290 nm are indicative of CO_2^+ emission. The positions of the atomic oxygen lines were corroborated using the NIST Atomic Spectra Database.[1]

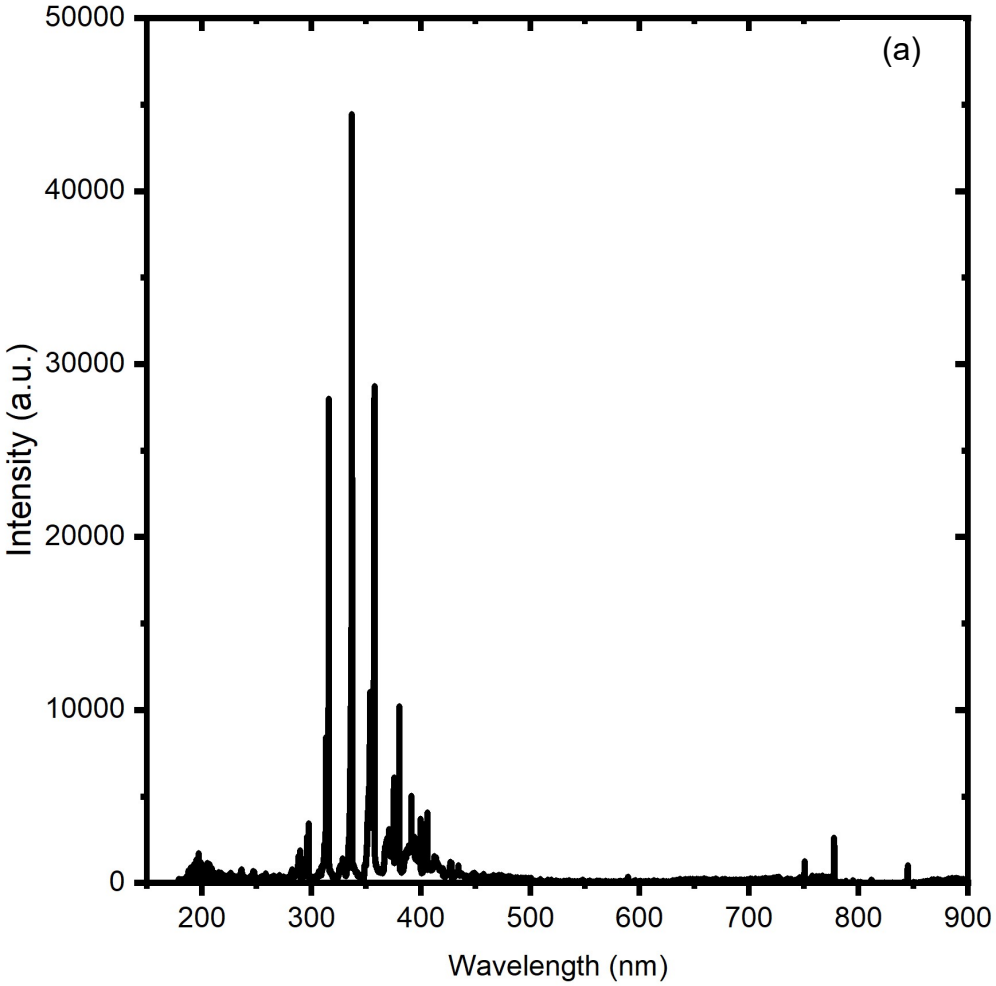

[1] Kramida, A., Ralchenko, Yu., Reader, J., and NIST ASD Team (2026). NIST Atomic Spectra Database (Version 5.14), [Online]. Available: https://physics.nist.gov/asd [Accessed: January 16, 2026].

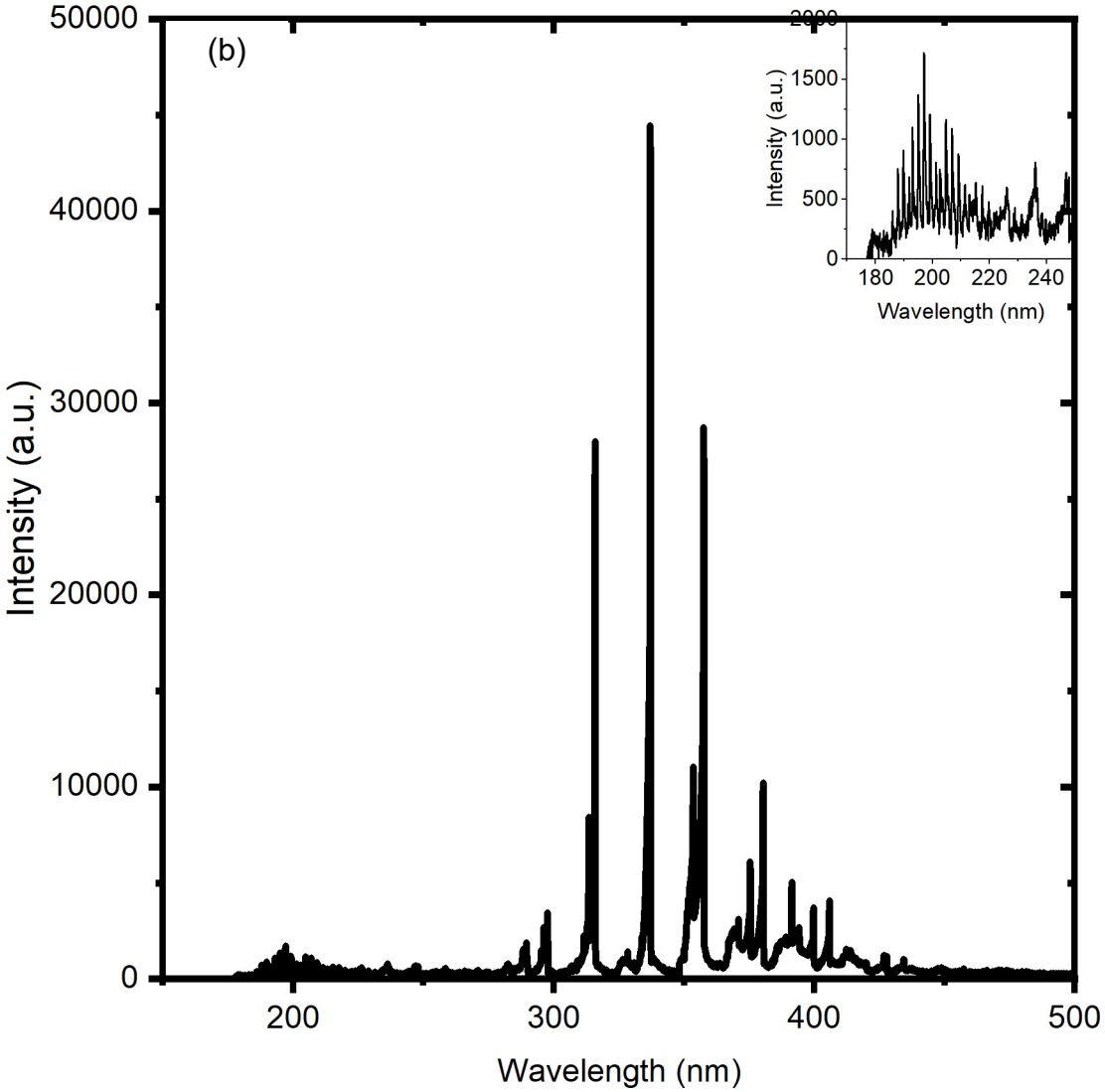

Figure S5: Optical emission spectrum of the non-thermal plasma generated by CO_2 dielectric barrier discharge (DBD) setup. (a) extended view and (b) zoom-in plot between 150 nm and 500 nm.

Table S1: Molecular diagnosis of CO_2 NTP DBD. Molecular and atomic emission assignments for the CO_2 DBD spectrum. The CO/CO_2^+ band assignments were based on the literature concerning CO_2 DBD OES, the and atomic line positions were cross-referenced with the NIST Atomic Spectra Database.

Wavelength (nm)	Intensity	Species	Transition	Line (nm)	Relative Intensity
189.798	910.716	O	3p' 5S°-4s' 5P	189.7102	355
189.798	910.716	O	3d ³D-3s' ³P°	189.8455	1
189.798	910.716	O	3p' ¹D-4f ¹F°	189.8603	270
189.798	910.716	O	3d ³D-3s' ³P°	189.8816	5
195.032	1370.72	O	3p ²P°-5d 4P	194.9376	1
195.032	1370.72	O	3p ²P°-5d 4P	194.9376	1
199.117	1206.16	O	3p 4P°-5s ²P	199.1658	0
206.869	1089.05	CO^+	X²Sig+-B²Sig+	206.78	100
206.869	1089.05	CO^+	X²Sig+-B²Sig+	206.79	100
206.869	1089.05	O_2^+	X²Pi(g)-A²Pi(u)	206.83	0
209.054	879.272	CO	X¹Sig+-A¹Pi	208.99	1000
209.054	879.272	CO^+	X²Sig+-B²Sig+	209.1	400
211.465	619.494	O	3p ²F°-3d ²D	211.528	2
211.465	619.494	O	4p ²P°-3p ²D	211.402	0

211.465	619.494	O	5d ²D- 6p ²P°	211.4435	213
211.465	619.494	O	5d ²D- 6p ²P°	211.4435	43
211.465	619.494	O	5d ²D- 6p ²P°	211.4837	387
288.408	1575.16	O	3p ³P-3d ³P°	288.3809	1
288.408	1575.16	O	3p ³P-3d ³P°	288.3856	2
288.408	1575.16	O	3d 4F- 5f 4F°	288.3912	9
288.408	1575.16	O	3d 4F-5fF ²[2]°	288.4221	0
288.408	1575.16	O	3d 4F- 5fF ²[4]°	288.4756	0
288.408	1575.16	CO_2^+	X²Pi-A²Sig+	288.4	0
311.57	2256.05	O	3p ³S-3d ³P°	311.5674	68
313.488	8420.49	O	3p 4D°-4s 4P	313.4213	113
313.488	8420.49	O	3p 4D°-4s 4P	313.4328	225
313.488	8420.49	O	3p 4D°-4s 4P	313.4726	136
313.488	8420.49	O	3p 4D°-4s 4P	313.4828	1077
313.488	8420.49	O	3p ²P-3d ²P°	313.507	40
313.488	8420.49	CO	a³Pi-b³Sig+	313.44	800
313.488	8420.49	CO_2^+	X²Pi-A²Pi	313.46	400

337.004	44460.9	O	3d 4F-5p 4D°	337.0293	11
337.004	44460.9	O	3p ^{3}S-3d ^{3}D°	336.9373	0
337.004	44460.9	CO_2^+	X^{2}Pi-A^{2}Pi	337	800
337.004	44460.9	O_2	X^{3}Sig-g-A^{3}Sig+u	337	1000
337.004	44460.9	O_2	X^{3}Sig-g-B^{3}Sig-u	337.01	1000
353.505	11069.6	O	3s' ^{3}P-3p'^{3}P°	353.4904	355
357.537	28744.5	O	3d ^{2}D-5p^{2}P°	357.4845	0
370.859	3132.8	O	3s' 5P-3p'5D°	370.9543	235
375.384	6103.35	O	3s ^{3}P°-3p^{3}D	375.4696	265
380.338	10235.7	O	3p ^{2}P°-4s^{2}P	380.2984	74
380.338	10235.7	O	3p ^{2}P°-4s^{2}P	380.3111	480
380.338	10235.7	O	3s 4P-3p^{2}D°	380.3137	0
391.324	5046.02	O_2	X^{3}Sig-g-B^{3}Sig-u	391.4	800
399.647	3738.35	CO^+	X^{2}Sig+-A^{2}Pi	399.73	900
405.771	4072.8	O	3s' ^{3}D-4p'^{3}D	405.7216	0
405.771	4072.8	O	3s' ^{3}D-4p'^{3}D	405.7281	1
405.771	4072.8	O	3s' ^{3}D-4p'^{3}D	405.8059	1

405.771	4072.8	O	3s' ^{3}D-4p'^{3}D	405.8517	1
750.495	2040.57	O	3d' ^{2}G-5f^{2}G°	750.4033	1
750.495	2040.57	O	3d' ^{2}G-5f^{2}G°	750.4708	49
844.688	2593.57	O	3s ^{3}S°-3p^{3}P	844.6247	115
844.688	2593.57	O	3s ^{3}S°-3p^{3}P	844.6359	574
844.688	2593.57	O	3s ^{3}S°-3p^{3}P	844.6758	345

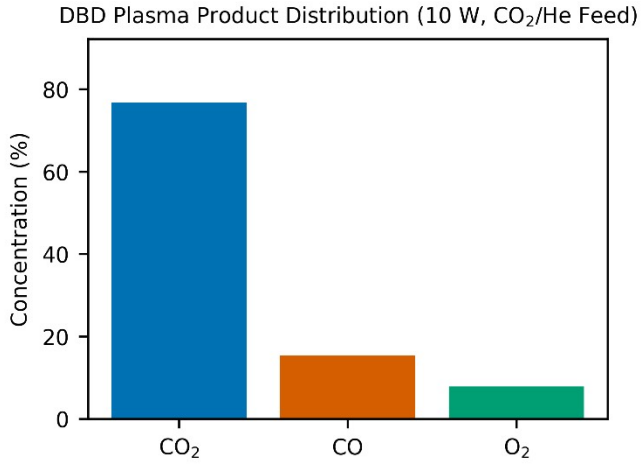

Figure S6: At a power of 10 W, the distribution of products from CO_2 NTP DBD was observed with a CO_2 flow rate of 30 NmL min^{-1} and an additional He flow of 5 NmL min^{-1}. No reactions driven by electrochemical processes were involved in this plot.

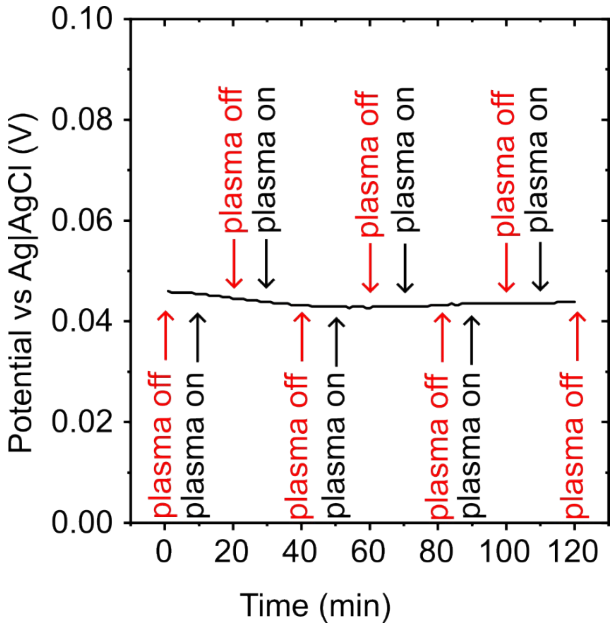

Figure S7: Open circuit voltage showing no effect of the plasma source on the electrochemical data.

S4: An electrochemical and product comparison between the performance of the electrolyser cell when the plasma source is switched on and off at different current densities for a fixed duration

Figs. S8-S12 compare the plasma-off and plasma-on voltage–current density responses of the electrolyte gap electrolyser over the current density range of 100 to 225 mA cm^{-2}. The cell voltage was consistently higher for plasma-off conditions, a theme that is evident across the various applied current experiments. For example, at 100 mA cm^{-2}, the cell voltage for the plasma-off experiment was 3.42 V. In contrast, the cell voltage during the plasma-on experiment was 2.58 V.

Fig. S8 shows the results of operating the electrolyte gap electrolyser at 100 mA cm^{-2}. In the plasma-off mode, after an induction period of *ca.* 1.5 – 2 s, a relatively stable cell voltage of 3.25 V (red line trace) is achieved, which then slowly drifts over 2600 s to up to ca. 3.45 V. When operating in plasma-on mode, a smaller cell voltage of 2.58 V is attained, which remains constant during the 1-hour experiment in Fig. S8 (black line trace).

In addition to the differences in operating cell voltage, differences were also observed in the product distribution and FE. Plasma-off resulted in carbon monoxide, methane, and ethylene (FE 64.74 ± 2.92%, 6.64 ± 0.60%, and 4.01 ± 0.55%, respectively) as the reaction products, along with hydrogen at an FE of 22.21 ± 1.63%, which was produced as a side reaction. The activation of CO_2 molecules by implementing a CO_2 plasma source and integrating it into the electrochemical cell resulted in the generation of both gaseous and liquid products. The primary gaseous products of the CO_2 plasma–electrochemical experiment were CO and ethylene, with yields of 23.59 ± 1.92% and 36.99 ± 1.06%, respectively. In addition, liquid products, including ethanol and acetate (C2 products), and formate (C1 product), with FE rates of 16.58 ± 1.51%, 4.83 ± 1.21%, and 8.41 ± 1.37%, respectively, were also generated. Furthermore, methane gas production disappeared, and the FE for H_2 decreased to 6.14%.

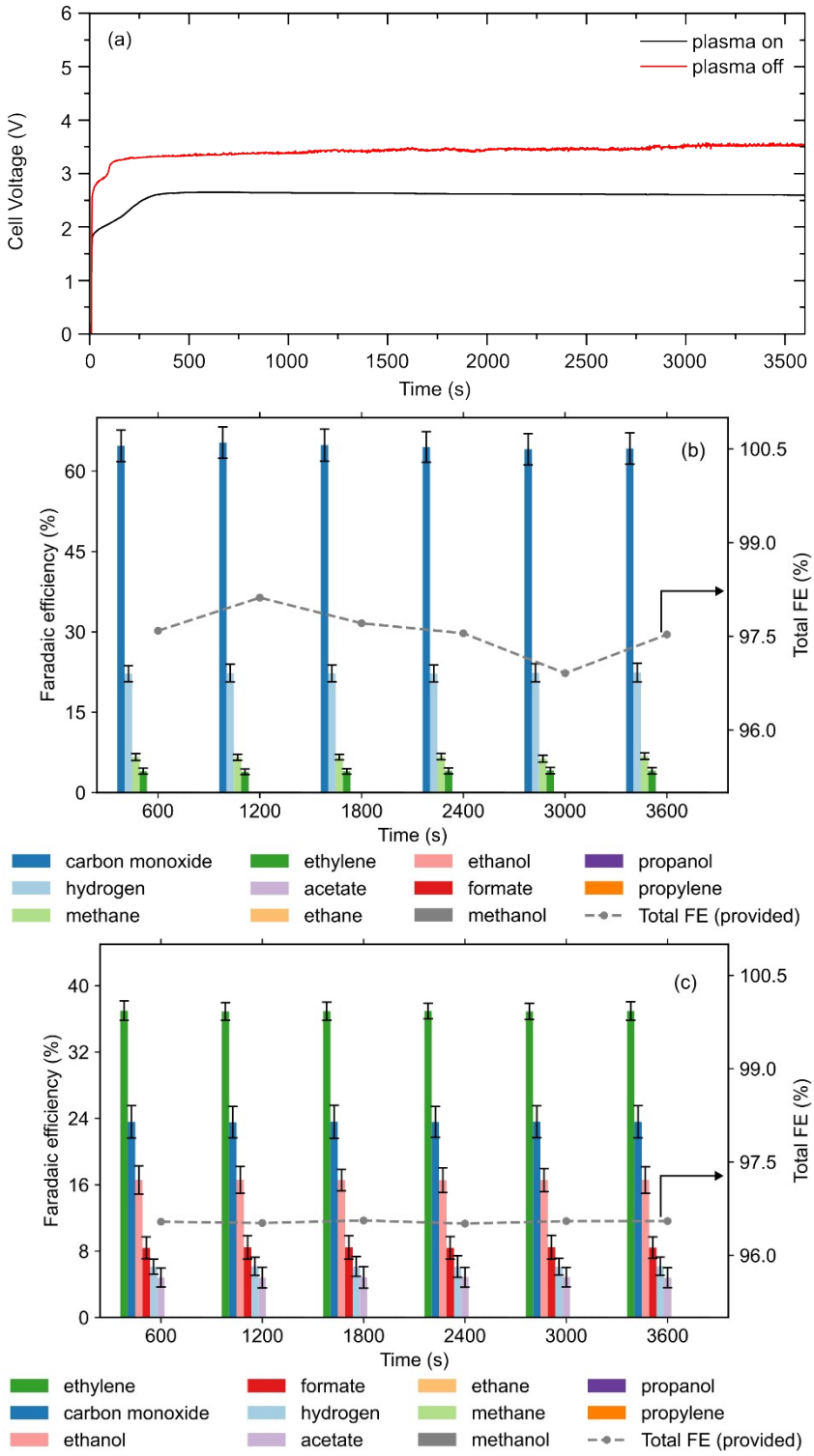

Figure S8: Galvanostatic experiments at 100 mA cm^{-2} using an electrolyte-gap electrolyser and 0.5 M $CsHCO_3$ + 0.25 M $Cs(SO_3CH_3)$ + 0.25 M Cs_2SO_4 aqueous electrolyte. Cell voltage **(a)** during the plasma-off (red) and CO_2 plasma-on (black) electrolysis of CO_2 and FE for gas and liquid products in plasma-off **(b)** and CO_2 plasma-on **(c)** modes.

1

Fig. S9 (a) compares the cell voltage profiles for CO_2 electroreduction under plasma-on and plasma-off conditions at a current density of 125 mA cm^{-2}. The cell voltage profile over time reveals a distinct difference between the two conditions. With plasma off (red line), the voltage remained relatively stable at approximately 3.86 V throughout the 3600 s. In contrast, the plasma-on condition (black line) shows a consistently lower voltage, which stabilises at approximately 2.86 V.

Fig. S9 (b) and (c) present the FEs of various CO_2 reduction products over time for plasma-off and plasma-on conditions, respectively. In the absence of plasma (Fig. S9 b), CO dominates the product distribution with FEs ranging from 60% to 65%, followed by H_2 (~20%–25%). Minor products such as methane, and ethylene appear in trace amounts, consistent with the competitive nature of the HER in conventional electrolysis

Under the plasma on (Fig. S9 (c)), a notable shift in product selectivity is observed, with the disappearance of methane. The FE of CO decreases significantly (~20–25%), while multi-carbon (C2+) products, such as ethylene, ethanol, and propanol, show marked increases, reaching FEs of ~40% for ethylene, for example.

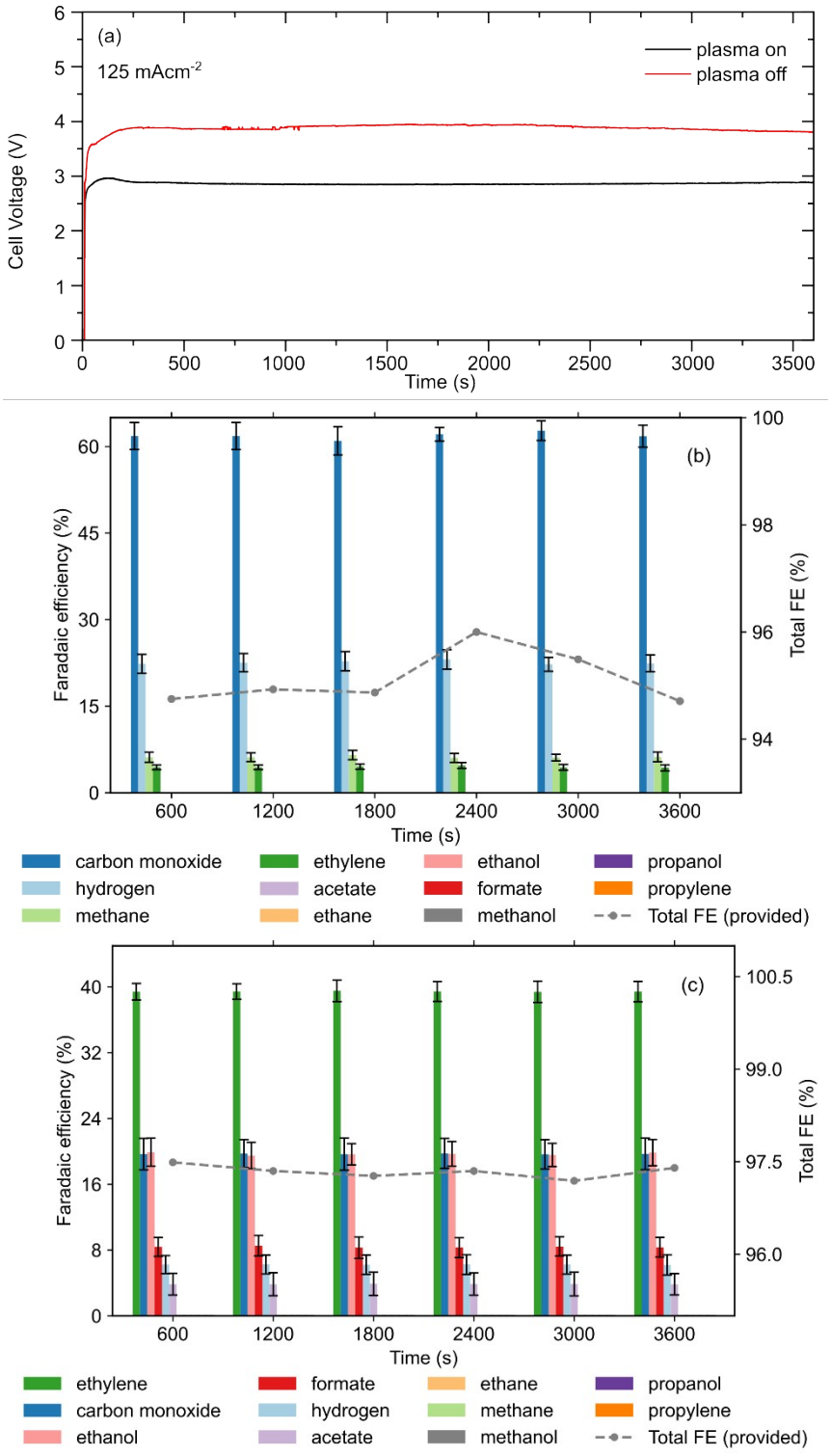

Figure S9: Galvanostatic experiments at 125 mA cm^{-2} using the electrolyte-gap electrolyser and 0.5 M $CsHCO_3$ + 0.25 M $Cs(SO_3CH_3)$ + 0.25 M Cs_2SO_4 aqueous electrolyte. Cell voltage (a) the plasma-off (red) and the CO_2 plasma-on (black) electrolysis of CO_2 and FE for gas and liquid products in plasma-off **(b)** and CO_2 plasma-on **(c)** modes.

1

Fig. S10 plots (a) illustrate the cell voltage profiles over time for the plasma-on and plasma-off conditions at a current density of 150 mA cm^{-2}. The plasma-on condition (black line) consistently exhibited a lower cell voltage. With plasma off (red line), the voltage value was approximately 4.12 V throughout the 3600 s duration. In contrast, the plasma-on condition (black line) showed a consistently lower voltage, which stabilised at approximately 2.97 V.

Fig. S10 (b) and (c) present the FEs of various CO_2 reduction products over time for the plasma-off and plasma-on conditions, respectively. In the plasma-off condition (Fig. S10 b), the dominant product is CO, with an FE ranging from ~50% to 60%, followed by H_2 (~20%–30%). Minor products, such as methane, ethylene, ethanol, and formate, are present in low quantities. This distribution reflects the typical challenge in CO_2 electroreduction, wherein the HER competes strongly with CO_2 reduction, especially at higher current densities. However, we notice the commencement of the production of liquid products, where ethanol is the main product with FE ~8%

In the plasma-on condition (Fig. S10 c), a significant shift in the product distribution was observed. The FE of H_2 decreased substantially, and methane was not produced, whereas the formation of multi-carbon products, such as ethylene, ethanol, and propanol, increased. Ethylene reached an FE of ~40–45%, indicating enhanced C–C coupling pathways. The total FE also appeared more stable and higher under plasma conditions, suggesting improved selectivity and utilisation of electrons toward C2 and C3 products.

1

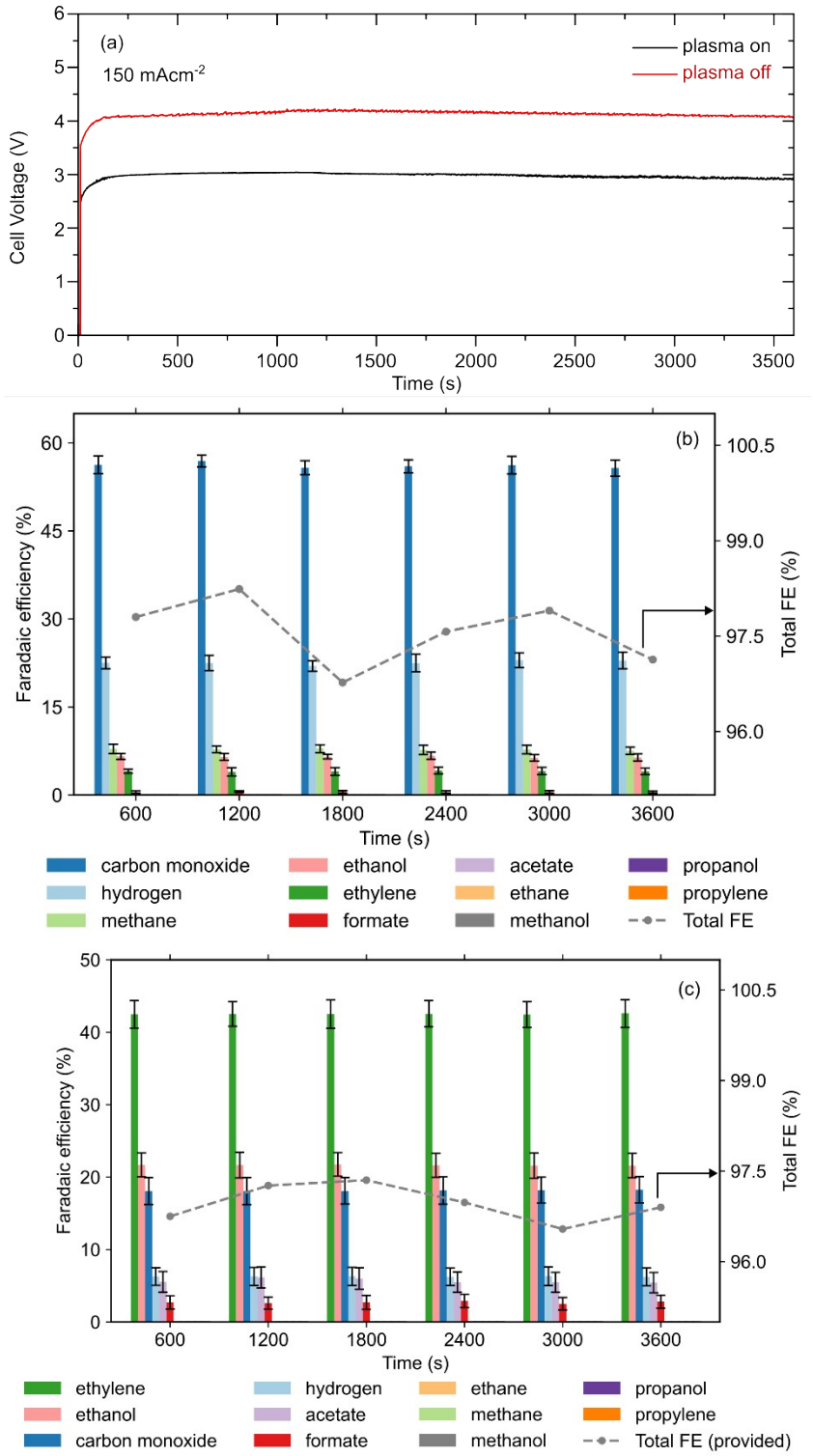

Figure S10: Galvanostatic experiments at 150 mA cm^{-2} using the electrolyte-gap electrolyser and 0.5 M $CsHCO_3$ + 0.25 M $Cs(SO_3CH_3)$ + 0.25 M Cs_2SO_4 aqueous electrolyte. Cell voltage (a) the plasma-off (red) and the CO_2 plasma-on (black) electrolysis of CO_2 and FE for gas and liquid products in plasma-off **(b)** and CO_2 plasma-on **(c)** modes.

Fig. S11 plot (a) shows the cell voltage profiles over time for the plasma-on and plasma-off conditions at a current density of 200 mA cm^{-2}. The plasma-on condition (black line) exhibited a lower cell potential. With plasma off (red line), the voltage registered was approximately 4.58 V throughout the 3600 s duration. In contrast, the plasma-on condition (black line) shows a consistently lower voltage of approximately 3.41 V.

Fig. S11 (b) and (c) present the FEs of various CO_2 conversion products over time for the plasma-off and plasma-on conditions, respectively. Under the plasma-off condition (b), the dominant product is CO, with an FE ranging from ~40% to 45%, followed by H_2 (~20%–30%). The drop in the FE of CO is accompanied by the formation of products such as methane, ethylene, ethanol, and formate. This distribution reflects the typical challenge in CO_2 electroreduction, wherein the HER competes strongly with CO_2 reduction, especially at higher current densities. Under the plasma-on condition (c), a significant shift in the product distribution is observed. The FE of H_2 decreases substantially, whereas the formation of multi-carbon products, such as ethylene, ethanol, formate, ethane, acetate, and propanol, increases. Ethylene has an FE of ~ 40 %–45% under these conditions.

1

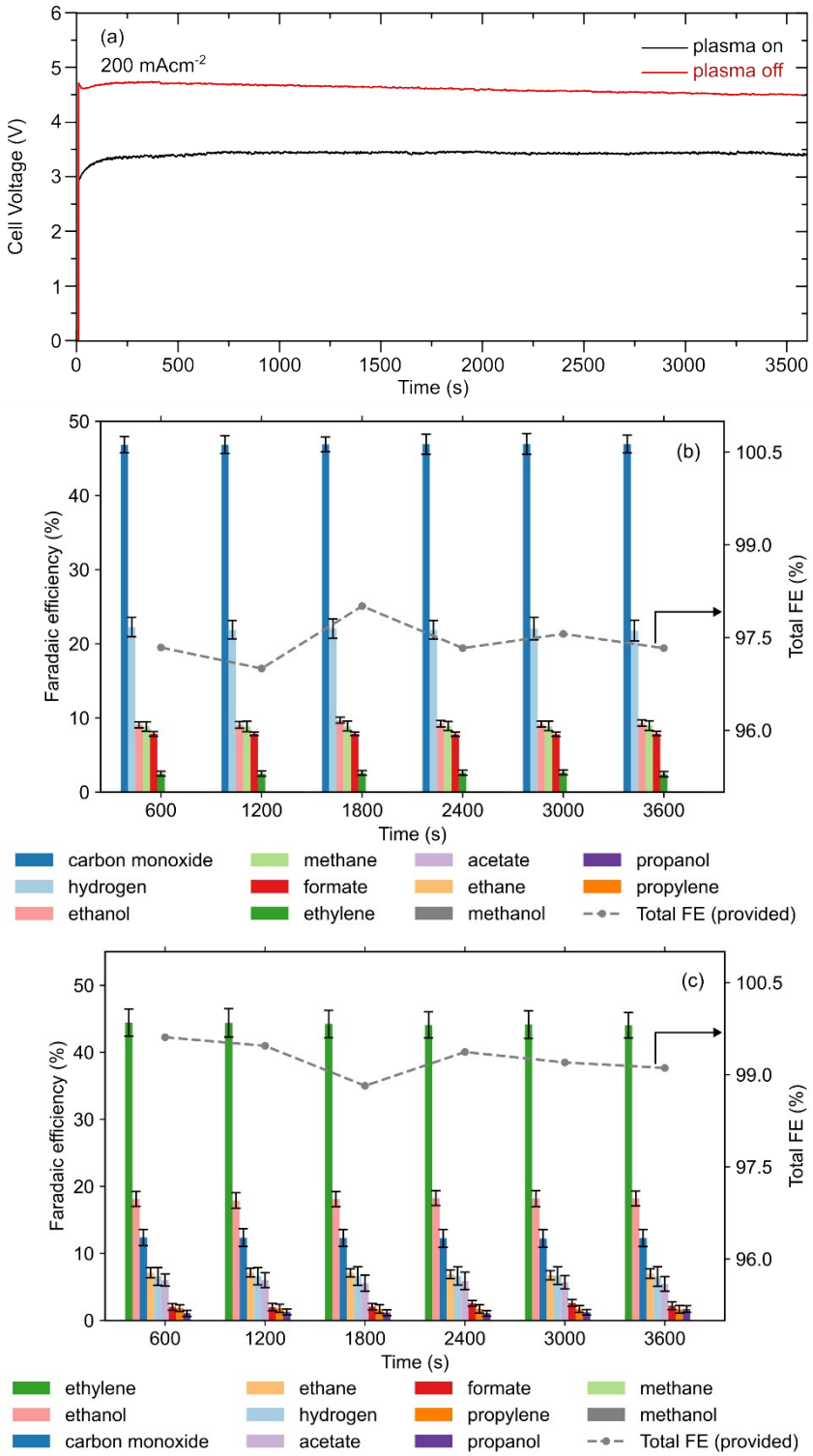

Figure S11: Galvanostatic experiments at 200 mA cm^{-2} using the electrolyte-gap electrolyser and 0.5 M $CsHCO_3$ + 0.25 M $Cs(SO_3CH_3)$ + 0.25 M Cs_2SO_4 aqueous electrolyte. Cell voltage (a) the plasma-off (red) and the CO_2 plasma-on (black) electrolysis of CO_2 and FE for gas and liquid products in plasma-off **(b)** and CO_2 plasma-on **(c)** modes.

1

Fig. S12 plot (a) shows the cell voltage profiles over time for the plasma-on and plasma-off conditions at a current density of 225 mA cm^{-2}. The plasma-on condition (black line) continues to exhibit a lower cell voltage. With plasma off (red line), the voltage registered is approximately 5.53 V throughout the 3600 s duration. In contrast, the plasma-on condition (black line) shows a consistently lower voltage of approximately 3.50 V.

Fig. S12 (b) and (c) present the FEs of various CO_2 conversion products over time under plasma-off and plasma-on conditions, respectively. Under the plasma-off condition (b), the dominant carbon product is CO, with an FE ranging from ~20% to 35%. H_2 reached (~30%–48%). The drop in the FE of CO is accompanied by the formation of products such as methane, ethylene, ethanol, and formate. Ethanol was the main liquid product during the plasma-off experiment, with an FE ranging between 15% and 30%. Under the plasma-on condition (c), a significant shift in the product distribution was observed. The FE of H_2 decreased substantially, whereas the formation of multi-carbon products, such as ethylene, ethanol, formate, ethane, acetate, and propanol, increased. Similar to the previous experiments, ethylene was the dominant product and reached an FE of ~42%–50%.

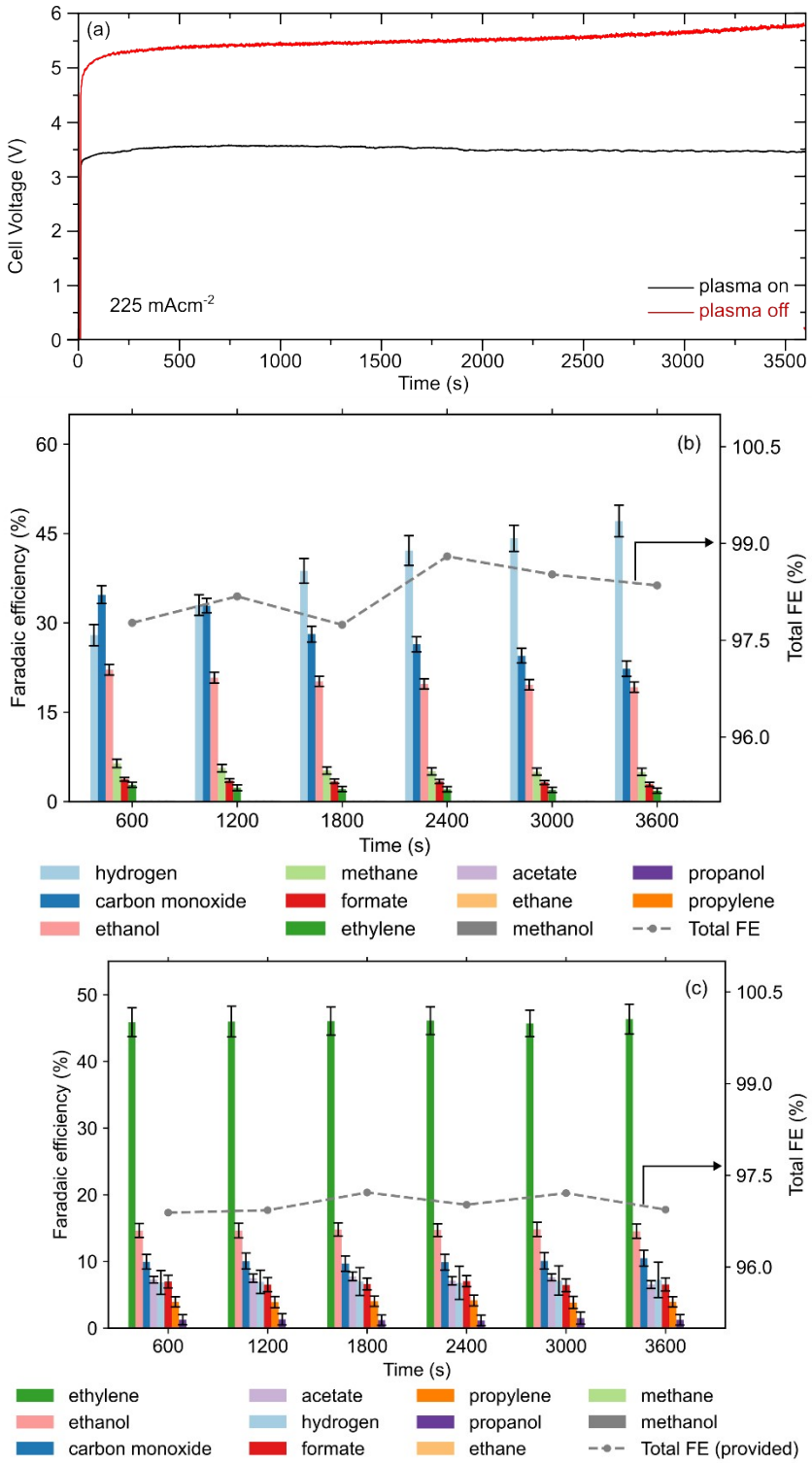

Figure S12: Galvanostatic experiments at 225 mA cm^{-2} using the electrolyte-gap electrolyser and 0.5 M $CsHCO_3$ + 0.25 M $Cs(SO_3CH_3)$ + 0.25 M Cs_2SO_4 aqueous electrolyte. Cell voltage (a) the plasma-off (red) and the CO_2 plasma-on (black) electrolysis of CO_2 and FE for gas and liquid products in plasma-off **(b)** and CO_2 plasma-on **(c)** modes.

1

Table S2 presents a comparison of the average cell voltage throughout the experiments, which were conducted for 1 h of electrolysis at each current density between 100 and 225 mA cm^{-2}. The trend exhibits a continued increase with increasing applied current density, resulting in a voltage difference that reaches $|\Delta E| = E_{plasma\text{-}off} - E_{plasma\text{-}on} = 2.03$ V at an applied current density of 225 mA cm^{-2}.

Table S2: the average of the cell voltage over 1 hour of electrolysis

	Plasma-off	**Plasma-on**	**Voltage difference (V)**
Current density (mA cm^{-2})	**Cell Voltage (V)**		
100	3.42	2.58	0.84
125	3.86	2.86	1
150	4.12	2.97	1.15
175	4.31	3.19	1.12
200	4.58	3.41	1.17
225	5.53	3.50	2.03

Figure S13: Image of the electrode after one hour of exposure to CO_2 NTP DBD experiments integrated with electrochemical reduction at 175 mA cm^{-2}.

S5: Faradaic and energy efficiency for gas and liquid products from CO_2 electrochemical conversion

Although faradaic efficiency (FE) serves as a direct measure of electron selectivity relative to total charge transfer, fluctuations in the rate of CO_2 conversion by plasma can introduce secondary effects on local reactant availability and gas-phase residence times. Specifically, these variations influence the lifetime and transport kinetics of transient, plasma-activated species as they migrate from the discharge zone to the GDE interface.

The FE of a product is calculated using the following general equation:

$$FE(\%) = \frac{Q_{prod}}{Q_{total}} \times 100 \qquad \text{Eq. S1}$$

Where $Q_{product}$ is the charge consumed to generate a specific product, and Q_{total} is the total charge passed during the reaction

The FE for each sampling interval Δt is:

$$FE(\%) = \frac{n_e F N_{product}}{I \Delta t} \times 100 \qquad \text{Eq. S2}$$

Where n_e is the number of electrons transferred per molecule of the product, *F* is the Faraday constant, $N_{product}$ is the amount of product (mol) formed during the sampling interval Δt and *I* is the current.

For gaseous products which was collected every 600 s (10 minutes)

$$N_{product} = x\ \Delta t \qquad \text{Eq. S3}$$

Where x is the molar flow rate mol min^{-1} measured for each product, and

$$x = \frac{v}{V_m}$$ Eq. S4

v is the normal flow rate (NL min^{-1}) at 25 ^{o}C and V_m is the molar volume (V_m = 24.46 L mol^{-1})

We employed an internal standard gas to measure gas products during CO_2 reduction. During CO_2 electrolysis, reactions consume carbon dioxide and produce various products at distinct stoichiometric ratios. For instance, the synthesis of one molecule of ethylene necessitates the consumption of two molecules of CO_2. Additionally, certain products, such as water, may condense and separate from the gas stream. Consequently, the total outlet flow rate is seldom identical to the total inlet flow rate. We introduced a known flow rate (5 NL/min) of an inert gas, nitrogen (N_2), into the collected gas stream. It is important to note that the N_2 line bypasses the electrochemical cell. As the internal standard gas does not undergo reactions at the electrodes and does not condense, its flow rate remains constant from the inlet to the outlet. We then find the exact volumetric flow rate of a product by multiplying the mole fraction of gas product measured by GC by the volumetric flow rate of the internal standard then by diving by the mole fraction of the internal standard measured by the GC *i.e.*

$$v = \frac{mole\ fraction\ of\ gas\ product\ \times\ volumetric\ flow\ rate\ of\ the\ internal\ st}{mole\ fraction\ of\ the\ internal\ standard}$$

. we then use v in eq. S4.

The liquid was collected in 600 s fractions. For liquid products quantified by UHPLC, $N_{product} = C_{product} \times V_{liquid}$, where $N_{product}$ is the moles of product formed during the sampling interval $\Delta t = 600\ s$, $C_{product}$ is the measured liquid concentration and V_{liquid} is the collected liquid volume for that 600 s fraction (catholyte outlet fraction + water trap fraction collected over the same interval).

$$FE_{liquid} = \frac{n_e F C_{product} V_{liquid}}{I \Delta t}$$ Eq. S5

Liquid-phase products were sampled at discrete 600 s intervals (∆t) by pooling effluents from both the catholyte outlet and the water trap. These quantities were quantified using ultra-high-performance liquid chromatography (UHPLC) with external calibration standards.

The total molar yield for each interval was calculated as the sum of the contributions from the catholyte and the trap. Faradaic efficiencies were subsequently determined based on the stoichiometric electron requirements for each specific CO_2 reduction pathway.

The full cell energy efficiency (EE) for plasma-off conditions is:[4]

$$EE_{product,plasma-off}(\%) = \frac{\Delta V_{thermo,product}}{\Delta V_{cell}} \times FE_{product} \times 100 \quad \text{Eq. S6}$$

$$\Delta V_{thermo,product} = \frac{\Delta G_{product}}{-nF} \quad \text{Eq. S7}$$

Where $^{\Delta V_{thermo,product}}$ is the thermodynamic cell voltage for the overall cell reaction of CO_2 with H_2O to give the product (CO, ethylene, ethane, ethanol, etc) and oxygen, $^{\Delta G_{product}}$ is the change in Gibbs free energy for that reaction, $^{\Delta V_{cell}}$ is the potential applied across the reactor, *F* is the Faraday constant, $^{FE_{product}}$ is the Faradaic efficiency for each product, and *n* is the number of electrons consumed to produce a specific product.

During the electrochemical conversion with plasma-on, the previously mentioned equation needs to be adjusted to account for the energy employed to create the plasma ($^{E_{plasma} = P_{plasma}t}$). Consequently, the plasma-on energy efficiency is:

$$EE_{product,plasma-on}(\%) = \frac{\Delta V_{thermo,product} I_{product}}{(\Delta V_{cell} I) + P_{plasma}} \times 100 \quad \text{Eq. S8}$$

In Fig. S14, plasma-off experiments are dominated by CO and methane, with limited formation of complex products. In contrast, plasma-on experiments led to a significant increase in ethylene, ethanol, and acetate, indicating enhanced C–C coupling and oxygenate formation.

The overall reaction combines the CO_2RR at the CuO cathode with the oxygen evolution reaction (OER) at the IrO_2 anode. The anodic half-reaction of IrO_2 in an aqueous solution is generally the OER:

Anode (Oxidation): $2H_2O \rightarrow O_2 + 4H^+ + 4e^-$

The cathodic half-reactions for the reduction of CO_2 to various products on CuO catalysts are as follows:

Target Product	Overall Balanced Cell Reaction
Carbon Monoxide (CO)	$2CO_2 \rightarrow 2CO + O_2$
Formate ($HCOOH$)	$2CO_2 + 2H_2O \rightarrow 2HCOOH + O_2$
Methane (CH_4)	$CO_2 + 2H_2O \rightarrow CH_4 + 2O_2$
Ethylene (C_2H_4)	$2CO_2 + 2H_2O \rightarrow C_2H_4 + 3O_2$
Ethanol (C_2H_5OH)	$2CO_2 + 3H_2O \rightarrow C_2H_5OH + 3O_2$
Acetate ($C_2H_3O_2^-$)	$2CO_2 + 2H_2O \rightarrow C_2H_3O_2^- + H^+ + 3O_2$

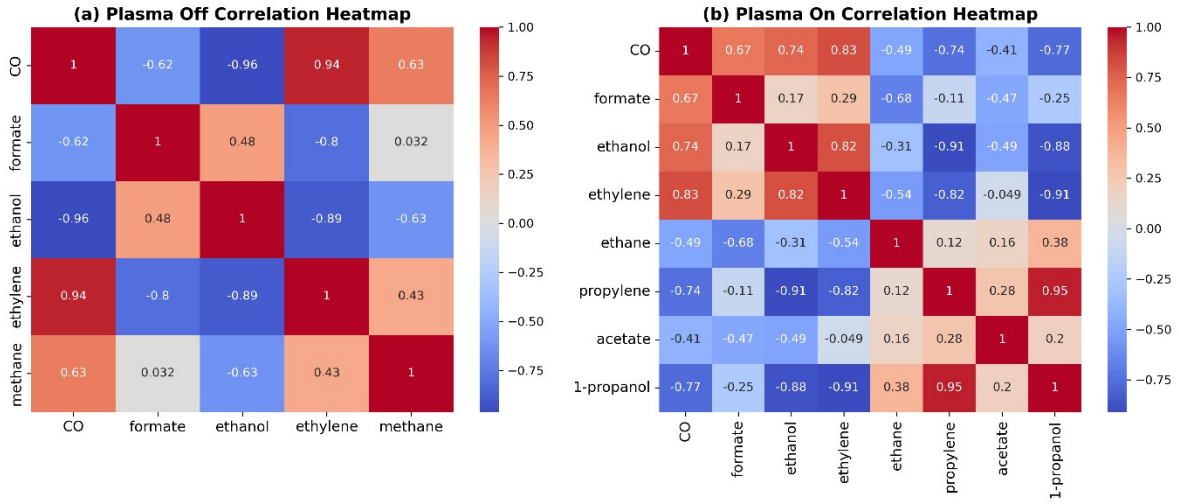

Figure S14: Correlation heatmap of gas and liquid products during (a) plasma-off and (b) plasma-on experiments at 175 mA cm^{-2}.

The correlation heatmap under plasma-off conditions shows a pronounced negative correlation between CO and ethanol, indicating that a decrease in CO is associated with an increase in ethanol. It also exhibits a positive correlation between methane and ethylene, suggesting analogous formation pathways. Under plasma-on conditions, the correlation heatmap reveals a strong positive correlation among ethylene, ethanol, and acetate, suggesting a shared or synergistic formation mechanism. Additionally, there is a negative correlation between CO and most C3 products, supporting the assertion that plasma alters the reaction pathway away from simple products.

S6: Carbon efficiency for gas products from CO_2 electrochemical conversion

Herein, we discuss the yield or carbon efficiency, *that is*, the ratio of CO_2 used in product formation to the number of moles of CO_2 that entered the cell. Equation 9 below is the general gas-phase formula for carbon efficiency.[4, 5]

It is defined as:

$$carbon\ efficiency\ gas\ (\%) = \left(\frac{\sum(n_x \times C_x)}{\left(n_{CO_{2,\,in}}\right)}\right) \times 100 \qquad \text{Eq. S9}$$

Where:

n_x is the number of moles of product x created

C_x is the number of carbons in products x

$n_{CO_{2,\,in}}$ is the number of moles of CO_2 that entered the cell

In the context of this study, carbon efficiency (%) refers to the carbon yield of the identified CO_2 reduction products relative to the total amount of CO_2 fed into the system. The CO_2 inlet flow was 30 NmL min^{-1}. Subsequently, we measured the outlet flow rate and product concentration using GC and HPLC, in conjunction with a flow meter at the outlet. We quantified the concentrations of gaseous and liquid products in terms of molar flow rates. All gas flow data were converted to molar flows using the ideal gas law, under the assumption of normal conditions (*i.e.*, 25 ˚C; some may refer to this condition as standard conditions more specifically in industry). Finally, we employed the aforementioned equation to calculate the carbon efficiency.

Example 1:

For plasma off condition and at 100 mA cm^{-2}, the applied current density for electrolysis,

The Molar flow of inlet CO_2 was calculated at normal (standard) conditions; hence, the temperature was 298.15 K (25 ^oC)

$n_{CO_{2,\,in}} = \frac{30}{24.46 \times 1000} =$ 0.03 NL min^{-1} ÷ 24.46 L mol^{-1} = 1.23 × 10^{-3} mol min^{-1}

Since samples were collected every 10 minutes, then $n_{CO_{2,\,in}}$ = 0.0123 mol

	2.01296 × 10^{-5}	2.01296 × 10^{-4}	1	2.01296 × 10^{-4}
	5.16142× 10^{-7}	5.16142× 10^{-6}	1	5.16142× 10^{-6}
	2.07286× 10^{-7}	2.07286× 10^{-6}	2	4.15× 10^{-6}

Total carbon gas product flow = 2.10 × 10^{-4} mol.

$carbon\ efficiency\ gas\ (\%)$ **=** (2.10 × 10^{-4} mol ÷ 0.0123 mol) × 100 = 1.71%.

Example 2:

For the plasma-on condition and at 100 mA cm^{-2}, the applied current density for electrolysis.

	7.33 × 10^{-6}	7.33 × 10^{-5}	1	7.33 × 10^{-5}
	0		1	0
	1.92× 10^{-6}	1.92× 10^{-5}	2	3.84× 10^{-5}

Total carbon gas product flow = 1.12 × 10^{-4} mol.

$carbon\ efficiency\ gas\ (\%)$ **=** (1.12 × 10^{-4} mol ÷ 0.0123 mol) × 100 = 0.91%.

Table S3: Gas phase carbon efficiency for plasma off and plasma on conditions

Current density (mA/cm^2)	**(Gas Phase) Carbon efficiency %**	
	Plasma Off	Plasma On
100	1.71	0.91
125	2.05	1.04
150	2.26	1.23
175	2.55	1.34
200	2.53	1.51
225	2.12	1.52

S7: Carbon efficiency for liquid products from CO_2 electrochemical conversion

Equation 10 is the liquid-phase formula for carbon efficiency, which is implemented; hence, we can complement the gas-phase carbon efficiency and close the system's carbon inventory.

$$carbon\ efficiency\ liquid\ (\%) = \left(\frac{\sum(n_c \times n_{product})}{n_{CO_2,\,in}}\right) \times 100 \qquad \text{Eq. S10}$$

Where:

- n_c is number of carbon atoms in the liquid product (*e.g.,* formate = 1, acetate = 2)
- $n_{product}$ is moles of each liquid product formed (mol)

The liquid product was tested by sampling and analysing the electrolyte (measured in catholyte + water trap) using HPLC. We used samples with known quantities of liquid products to generate calibration curves, which were then used to determine the concentration and total moles of each liquid product.

Table S4: Liquid carbon efficiency for plasma off and plasma on conditions

Current density (mA cm^{-2})	**(Liquid Phase) Carbon efficiency %**	
	Plasma Off	Plasma On
100	0	0.41
125	0	0.53
150	0.11	0.48
175	0.14	0.53
200	0.55	0.58
225	0.63	0.91

S8: Carbon efficiency for carbonate and bicarbonate products from CO_2 electrochemical conversion

We used a titration method to directly measure carbonate and bicarbonate. We performed a two-step acid titration using 0.1 M HCl to differentiate carbonate (CO_3^{2-}) and bicarbonate (HCO_3^-). The first endpoint at pH ~8.3 is the neutralisation of CO_3^{2-} to HCO_3^-, and the second endpoint at pH ~4.5 is the neutralisation of HCO_3^- to CO_2; we then calculated the concentrations using stoichiometry and titrant volume. These results were further confirmed by ion chromatography analysis. Samples were filtered through 0.45 µm membranes to remove particulates and avoid CO_2 uptake or loss and, if necessary, diluted in the eluent to minimise baseline artefacts. Separation was achieved on a Dionex IonPac AS4A-SC (or AS14) column using a dilute carbonate/bicarbonate eluent (~1.7–1.8 mM $NaHCO_3/Na_2CO_3$), with chemical suppression for conductivity detection and quantification employing multi-point calibration. Tables S5–S7, the pH values reported in Tables S6–S7 correspond to the outlet pH measured at the cell exit.

Table S5: Carbon efficiency for the conversion of CO_2 to carbonate and bicarbonate

Current density (mA/cm^2)	***(carbonate and bicarbonate) Carbon efficiency %***	
	Plasma Off	Plasma On
100	0.011	0.01
125	0.015	0.013
150	0.019	0.015
175	0.022	0.017
200	0.024	0.02
225	0.027	0.022

Table S6: Concentration of carbonate and bicarbonate for plasma on mode experiments

Current	**Plasma**	**pH ***	**HCO_3^-**	**CO_3^{2-}**	**Total Carbonate**

Density (mA/cm²)	Mode		(mmol)	(mmol)	(mmol)
100	On	7.5	0.11	0.02	0.13
125	On	7.8	0.12	0.03	0.16
150	On	8.1	0.14	0.04	0.19
175	On	8.5	0.16	0.06	0.22
200	On	8.9	0.17	0.07	0.25
225	On	9.2	0.19	0.08	0.28
*pH value at the exit of the electrolyte from the cathode compartment ** point of entry pH is 7.8					

Table S7: Concentration of carbonate and bicarbonate for plasma off-mode experiments

Current Density (mA/cm²)	Plasma Mode	pH *	HCO_3^- (mmol)	CO_3^{2-} (mmol)	Total Carbonate (mmol)
100	Off	8.2	0.09	0.04	0.14
125	Off	9	0.11	0.06	0.18
150	Off	9.5	0.13	0.09	0.23
175	Off	10.2	0.15	0.11	0.27
200	Off	10.8	0.17	0.12	0.30
225	Off	11.3	0.18	0.13	0.33
*pH value at the exit of the electrolyte from the cathode compartment ** point of entry pH is 7.8					

S9: Carbon efficiency for all products from CO_2 electrochemical conversion

The carbon balance is accounted for as follows. Unreacted CO_2: The majority of the carbon balance is unconverted CO_2 that exits the reactor. This is common in flow-cell electrolysis, where high flow rates are used to maintain a stable triple-phase boundary. Carbonate and Bicarbonate Formation: A significant portion of the CO_2 is not electrochemically reduced but is instead chemically absorbed into the alkaline or neutral electrolyte. As indicated in the pH data/table, the total carbonate/bicarbonate concentration in the electrolyte increases during operation, reaching up to 0.33 mmol. This "parasitic" carbon capture process consumes CO_2 without yielding the intended fuels. *Dissolved Products: A minor fraction of gaseous products, such as CO or volatile liquids, may remain dissolved in the electrolyte or become trapped in the gas diffusion electrode (GDE) assembly, slightly reducing the recovery values.*

Table S8: sum of all products carbon efficiency by the sum of gas, liquid, carbonate and bicarbonate products

Current density (mA/cm^2)	**Sum of Carbon efficiency %**	
	Plasma Off	Plasma On
100	1.86	1.33
125	2.24	1.58
150	2.51	1.73
175	2.84	1.88
200	2.85	2.11
225	2.47	2.45

References

1. G. Leonzio, A. Hankin and N. Shah, *Chemical Engineering Research and Design*, 2024, **208**, 934-955.
2. J. M. Yoo, J. Ingenmey, M. Salanne and M. R. Lukatskaya, *Journal of the American Chemical Society*, 2024, **146**, 31768-31777.
3. S. Soldatov, G. Link, L. Silberer, C. M. Schmedt, E. Carbone, F. D'Isa, J. Jelonnek, R. Dittmeyer and A. Navarrete, *ACS Energy Letters*, 2021, **6**, 124-130.
4. D. Wakerley, S. Lamaison, J. Wicks, A. Clemens, J. Feaster, D. Corral, S. A. Jaffer, A. Sarkar, M. Fontecave, E. B. Duoss, S. Baker, E. H. Sargent, T. F. Jaramillo and C. Hahn, *Nature Energy*, 2022, **7**, 130-143.
5. S. Garg, Q. C. Xu, A. B. Moss, M. Mirolo, W. Y. Deng, I. Chorkendorff, J. Drnec and B. Seger, *Energy & Environmental Science*, 2023, **16**, 1631-1643.